

# Noise pre-filtering techniques in fluorescence-enhanced optical tomography

B. Zhu,<sup>1</sup> M. J. Eppstein,<sup>2</sup> E. M. Sevick-Muraca,<sup>3</sup> A. Godavarty<sup>1\*</sup>

<sup>1</sup>*Optical Imaging Laboratory, Department of Biomedical Engineering, Florida International University, Miami, Florida, 33174*

<sup>2</sup>*Department of Computer Science, University of Vermont, Burlington, VT, 05405*

<sup>3</sup>*Department of Radiology, Baylor College of Medicine, Houston, TX, 77030*

\*Corresponding author: [godavart@fiu.edu](mailto:godavart@fiu.edu)

**Abstract:** In this contribution, different measurement noise pre-filtering techniques were developed using frequency-domain fluorescence measurements of homogeneous breast phantoms. We demonstrated that implementing noise pre-filtering, based on modulation depth and measurement error in amplitude, can improve model match between experimental and simulated data under varying experimental conditions (target depths, 1-3 cm and fluorescence optical contrast, 1:0 and 100:1). Noise pre-filtering also improves the qualitative estimation of target(s) location in reconstructed images in deep target(s) when there was fluorescence in the background. Interestingly, decreases in model mismatch did not necessarily correlate with increases in reconstructed target accuracy. In addition, it was observed that pre-filtering measurement noise using different criteria can help differentiate target(s) from artifacts, thus possibly minimizing the false-positive cases in a clinical environment.

©2007 Optical Society of America

**OCIS codes:** (260.2510) Fluorescence; (100.6950) Tomographic imaging processing; (110.4280) Noise in imaging systems

---

## References and links

1. M. A. Franceschini, K. T. Moesta, S. Fantini, G. Gaida, E. Gratton, H. Jess, W. W. Mantulin, M. Seeber, P. M. Schlag, and M. Kaschke, "Frequency-domain techniques enhance optical mammography: Initial clinical results," *Proc. Natl. Acad. Sci. USA* **94**, 6468-6473 (1997).
2. S. Fantini, S. A. Walker, M. A. Franceschini, M. Kaschke, P. M. Schlag, and K. T. Moesta, "Assessment of the size, position, and optical properties of breast tumors in vivo by noninvasive optical methods," *Appl. Opt.* **37**, 1982-1989 (1998).
3. K. T. Moesta, S. Fantini, H. Jess, S. Totkas, M. A. Franceschini, M. Kaschke, and P. M. Schlag, "Contrast features of breast cancer in frequency-domain laser scanning mammography," *J. Biomed. Opt.* **3**, 129-136 (1998).
4. D. Grosenick, H. Wabnitz, H. H. Rinneberg, K. T. Moesta, and P. M. Schlag, "Development of a time-domain optical mammograph and first in vivo applications," *Appl. Opt.* **38**, 2927-2943 (1999).
5. S. B. Colak, M. B. van der Mark, G. W. 't Hooft, J. H. Hoogenraad, E. S. van der Linden, and F. A. Kuijpers, "Clinical Optical Tomography and NIR Spectroscopy for Breast Cancer Detection," *IEEE J. Sel. Top. Quantum Electron.* **5**, 1143-1158 (1999).
6. B. W. Pogue, S. P. Poplack, T. O. McBride, W. A. Wells, K. S. Osterman, U. L. Osterberg, and K. D. Paulsen, "Quantitative hemoglobin tomography with diffuse near-infrared spectroscopy: Pilot results in the breast," *Radiology* **218**, 261-266 (2001).
7. H. Jiang, Y. Xu, N. Iftimia, J. Eggert, K. Klove, L. Baron, and L. Fajardo, "Three-dimensional optical tomographic imaging of breast in a human subject," *IEEE Trans. Med. Imaging* **20**, 1334-1340 (2001).
8. A. Li, G. Boverman, Y. Zhang, D. Brooks, E.L. Miller, M.E. Kilmer, Q. Zhang, E.M. Hillman, and D.A. Boas, "Optimal linear inverse solution with multiple priors in diffuse optical tomography," *Appl. Opt.* **44**, 1948-56 (2005).
9. Q. Zhang, T.J. Brukilacchio, A. Li, J.J. Stott, T. Chaves, E. Hillman, T. Wu, M.Chorlton, E. Rafferty, R.H. Moore, D.B. Kopans, and D.A. Boas, "Coregistered tomographic x-ray and optical breast imaging: initial results," *J. Biomed. Opt.* **10**, 24033(2005).

10. A.P. Gibson, J.C. Hebden, and S.R. Arridge, "Recent advances in diffuse optical imaging," *Phys. Med. Biol.* **50**, R1-43 (2005).
11. V. Ntziachristos, C.-H. Tung, C. Bremer, and Weissleder, "Fluorescence molecular tomography resolves protease activity *in vivo*," *Nat. Med.* **8**, 757-760 (2002).
12. E. E. Graves, J. Ripoll, R. Weissleder, and V. Ntziachristos, "A submillimeter resolution fluorescence molecular imaging system for small animal imaging," *Med. Phys.* **30**, 901-911 (2003).
13. G. Zacharakis, J. Ripoll, R. Weissleder, and V. Ntziachristos, "Fluorescent protein tomography scanner for small animal imaging," *IEEE Trans. Med. Imaging* **24**, 878-885 (2005).
14. A. Godavarty, M. J. Eppstein, C. Zhang, S. Theru, A. B. Thompson, M. Gurfinkel, E. M. Sevick-Muraca, "Fluorescence-enhanced optical imaging in large tissue volumes using a gain-modulated ICCD camera," *Phys. Med. Biol.* **48**, 1701-1720 (2003).
15. A. Godavarty, A. B. Thompson, R. Roy, M. Gurfinkel, M. J. Eppstein, C. Zhang, E. M. Sevick-Muraca, "Diagnostic imaging of breast cancer using fluorescence-enhanced optical tomography: phantom studies," *J. Biomed. Opt.* **9**, 488-496 (2004).
16. A. Godavarty, C. Zhang, M. J. Eppstein, E. M. Sevick-Muraca, "Fluorescence-enhanced optical imaging of large phantoms using single and simultaneous dual point illumination geometries," *Med. Phys.* **31**, 183-190 (2004).
17. A. Godavarty, E. M. Sevick-Muraca, M. J. Eppstein, "Three-dimensional fluorescence lifetime tomography," *Med. Phys.* **32**, 992-1000 (2005).
18. Y. Chen, X. Intes, B. Chance, "Development of high-sensitivity near-infrared fluorescence imaging device for early cancer detection," *Biomed. Instrum. Technol.*, **39**, 75-85 (2005).
19. Z. Sun, Y. Huang, E. M. Sevick-Muraca, "Precise analysis of frequency domain migration measurement for characterization of concentrated colloidal suspensions, *SCI. Instrum.* **73**, 383-393(2002)
20. O. C. Zeinkiewicz, and R. L. Taylor. *The Finite Element Methods In Engineering Science* (McGraw-Hill, New York, 1989).
21. J. N. Reddy. *An Introduction to the Finite Element Method* 2ed. (McGraw-Hill, New York, 1993).
22. M. J. Eppstein, D. E. Dougherty, T. L. Troy, and E. M. Sevick-Muraca, "Biomedical optical tomography using dynamic parameterization and Bayesian conditioning on photon migration measurements", *Appl. Opt.*, **38**:2138-2150 (1999).
23. M. J. Eppstein, D. J. Hawrysz, A. Godavarty, and E. M. Sevick-Muraca, "Three-dimensional, near-infrared fluorescence tomography with Bayesian methodologies for image reconstruction from sparse and noisy data sets," *Proc. Natl. Acad. Sci. USA* **99**, 9619-9624 (2002).

## 1. Introduction

Optical imaging is based on the principle of using the minimally absorbed and preferentially scattered near-infrared (NIR) light (between the wavelengths of 700-900 nm) in order to illuminate and detect optical signals deep into the tissue surface [1-10]. The inherent differences in the optical properties (in terms of absorption and scattering coefficient) between normal and diseased tissues detected using optical imaging technique is not sufficient for diagnosing early-stage or small volume tumors. Hence, contrast agents are used to improve the optical contrast ratio from small volume or deeply located targets.

Over the past few years, several researchers have embarked on the development of fluorescence-enhanced NIR optical technology as a new modality for molecularly based diagnostic imaging in deep tissues. Three-dimensional (3-D) fluorescence tomography studies have been successfully demonstrated by various research groups on small animal models [11-13] and recently on large tissue phantoms [14-18]. In all these tomography studies, the 3-D reconstructed images of the tissue phantoms are typically contaminated with artifacts (noise in parameter estimates) apart from the reconstructed target(s). These artifacts can arise from one or more of the following: (i) experimental errors arising from estimated tissue background optical properties, and/or homogeneity of the background phantom; (ii) instrumentation errors arising from detectors (based on their precision), optical filters (from light leakage), or other electronics that contaminate the NIR signal; and (iii) computational errors arising from the approximation of the light propagation models used in reconstruction algorithms or the accuracy of the numerical techniques employed in solving the highly ill-posed optical tomography problem. Efforts are made in minimizing the errors during experimental studies and data acquisition, although errors remain and appear as artifacts in the reconstructed images.

To date, there is little emphasis by researchers on the methods (if) implemented to pre-filter their noisy data prior to tomography studies [14-17]. In recent 3-D fluorescence optical tomography studies performed by Godavarty *et al* [14], a modulation depth based noise pre-filtering technique was employed to remove noisy measurement prior to image reconstructions. A modulation depth (AC/DC) based pre-filtering technique was chosen because model mismatch errors (errors between experimental and simulated data, which is obtained from appropriate light propagation models) were observed to increase sharply at detection points whose modulation depth was below 0.025 [14]. Noisy measurements may also exist independent of increased model mismatch errors, and thus remain unfiltered using the modulation depth pre-filtering criterion. These unfiltered measurements may in turn contaminate the 3-D reconstructed images with artifacts. Hence, in this contribution, different noise pre-filtering techniques are developed (which also includes the modulation depth based pre-filtering criteria from past studies) using experimental studies. The effect of filtering noisy optical measurements on 3-D image reconstructions is studied. Initially, the instrumentation and the different experimental data sets employed in our studies are briefly described. The correlations among different measurement parameters (that contain noise), such as modulation depth, measurement errors in amplitude (AC) and phase shift ( $\theta$ ) value, and source-detector distance are investigated in order to develop different noise pre-filtering techniques. Three-dimensional (3-D) image reconstructions using the developed noise pre-filtering techniques are presented under different experimental cases (1:0 and 100:1 target:background fluorescence absorption contrast) at varying target depths. The effect of implementing the developed noise pre-filtering on model mismatch errors and quality of 3-D image reconstructions is discussed.

## 2. Materials and methods

### 2.1 Instrumentation

A frequency-domain photon migration (FDPM) intensified CCD (ICCD) based optical imaging system was developed in order to perform fluorescence-enhanced optical imaging on large breast phantoms [14]. The schematic of the FDPM-ICCD imaging system is illustrated in Fig. 1. Detailed description of the instrumentation is provided elsewhere [14] and is briefly described herein.

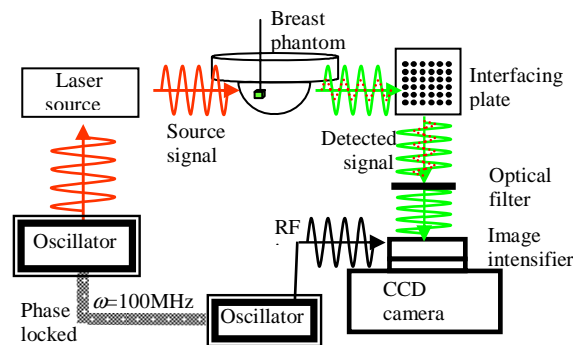


Fig. 1. Schematic of the instrumentation set-up of the FDPM-ICCD imaging system

Sinusoidally modulated NIR light source at 783nm wavelength and at 100MHz was used to sequentially illuminate the hemispherical surface of the breast phantom at multiple point locations (via optical fibers). The generated fluorescent signals (from the external fluorescence contrast agents used in the phantom) along with the attenuated excitation signals (at 100 MHz) were collected via optical fibers from the hemispherical surface of the phantom and imaged using the ICCD camera, which was also modulated at 100MHz. Appropriate

optical filters (band pass, long pass, holographic filters, [14]) were used to eliminate the strong excitation signal, allowing only the weak fluorescence signal to be imaged by the ICCD detector. The two oscillators modulating the light at both the source and detector ends were phase locked, causing the steady-state signal, acquired and stored by the CCD camera, to be phase-sensitive.

By introducing a phase delay varying from 0 to  $2\pi$  between the two oscillators, steady-state phase sensitive measurements were observed to vary sinusoidally. Upon performing Fast Fourier Transforms (FFT), the amplitude (AC) and phase shift ( $\theta$ ) at each pixel (or point) was extracted for each repeated measurement (five in this case). Measurement repetitions were performed for each point detector location in order to assess the measurement error of the imaging instrument.

The integration time of the CCD camera was varied for different experimental cases, and even within each experimental case, based on the distance between the point of illumination and detection. The change in integration time can impact the inherent sources of noise in the imaging system (i.e. shot noise and electronic noise). In order to remove these sources of noise (when dominant and obvious over the weak fluorescence measurements) for our studies, a criteria was implemented to determine which fluorescence measurements should even be recorded during data acquisition. The criteria used was that fluorescence measurements for a given point source illumination was recorded only if the average modulation depth of all the collection points on the interfacing plate (that is imaged by the CCD camera) was greater than 0.1. This criterion was based on various preliminary studies with and without the use of fluorescence, in order to differentiate the actual measurements from the obvious/dominant noise (only) arising from the imaging system.

## 2.2 Experimental parameters

Initially, experiments were performed under homogeneous conditions (i.e. no target present) in order to determine any correlations among different measurement parameters (described in Section 2.3) and in turn develop different noise pre-filtering techniques. These techniques were further used for different heterogeneous phantoms contains target(s) under different experimental conditions. For homogeneous studies, the hollow breast phantom was filled

Table 1 Optical properties of the background phantom during the homogeneous phantom study

Optical properties ( $\text{cm}^{-1}$ )		Background
Excitation	$\mu_{axf} + \mu_{axi}$	0.003+0.0231
	$\mu_{sx}'$	9.99
Emission	$\mu_{amf} + \mu_{ami}$	0.0005+0.0292
	$\mu_{sm}'$	9.67

$\mu_{axf}, \mu_{amf}$ : Absorption coefficient due to the fluorophores at excitation and emission wavelengths, respectively.

$\mu_{axi}, \mu_{ami}$ : Intrinsic absorption coefficient of 1% Liposyn solution at excitation and emission wavelengths, respectively.

$\mu_{sx}', \mu_{sm}'$ : Reduced scattering coefficient of 1% Liposyn solution at excitation and emission wavelengths, respectively.

with 0.01  $\mu\text{M}$  Indocyanine Green (ICG, an external fluorescence contrast agent) in 1% Liposyn solution (Abbott Laboratories, North Chicago, IL). The intrinsic optical properties of 1% Liposyn in the homogeneous phantom were measured using a single-pixel FDPM imaging system [19] and the absorption coefficient of the ICG was estimated from its concentrations (see Table 1).

Further experimental studies were performed under target: background fluorescence absorption contrast ratios of 1:0 and 100:1 using a single  $1 \times 1 \times 1 \text{ cm}^3$  target, which was located

~ 1 to 3 cm deep from the phantom surface. One  $\mu\text{M}$  of ICG in 1% Liposyn solution was used in the target, with 0 and 0.001  $\mu\text{M}$  ICG in the 1% Liposyn background, for the perfect (1:0) and imperfect (100:1) uptake cases, respectively, and for all the target depths (1.4, 2.0 and 2.8 cm). The optical properties of the target and the background for different experimental cases (using a different batch of 1% Liposyn solution from the homogeneous phantom studies) are provided in Table 2.

Table 2 Optical properties of target and background for different contrast ratio experiments and for all the target depth studies.

Optical Properties ( $\text{cm}^{-1}$ )		Perfect Uptake (1:0)		Imperfect uptake (100:1)	
		Target	Background	Target	Background
Excitation	$\mu_{axf} + \mu_{axi}$	0.300+0.0248	0.000+0.0248	0.300+0.0248	0.003+0.0248
	$\mu_{sx}$	10.88	10.88	10.88	10.88
Emission	$\mu_{amf} + \mu_{ami}$	0.050+0.0322	0.000+0.0322	0.050+0.0322	0.0005+0.0322
	$\mu_{sm}$	9.82	9.82	9.82	9.82

### 2.3 Correlation studies among different measurement parameters

Frequency-domain measurements provide AC and phase shift ( $\theta$ ) information for different source-detector pairs and distances (see Fig. 2). These measurements can in turn be used to calculate the DC, modulation depth (AC/DC), measurement errors in AC and  $\theta$  (i.e. standard deviations in repeated AC and  $\theta$  measurements). Image reconstructions employ one or more of the above measurement parameters in order to reconstruct the 3-D optical property distribution map of the phantom, and eventually determine the target(s)' location and size. The quality of image reconstructions may improve by differentiating noise from the actual optical signal, prior to inversions. Hence, noise pre-filtering techniques are developed and implemented prior to image reconstructions.

Noise pre-filtering can be implemented by using cut-off limits in AC,  $\theta$ , DC, AC/DC, and/or measurement errors in AC and  $\theta$ . However, these measurement parameters could possibly be independent or dependent on each other, or with respect to changes in source-detector distance. Correlation among these parameters can aid in reducing the number of noise pre-filtering criteria, since filtering noisy data from one measurement parameter will eliminate the same noisy data from its correlated parameter.

In the current study, correlation studies were performed among the following measurement parameters: (i) modulation depth; (ii) source-detector distance; (iii) phase shift ( $\theta$ ); (iv) measurement error in AC (standard deviation of normalized repeated AC measurements); and (v) measurement error in  $\theta$  (standard deviation of normalized repeated  $\theta$  measurements). Since the measurement parameters AC and DC are contained in modulation depth (AC/DC), they were used as a single parameter in the correlation studies. The selection of the standard deviations is due to its statistical characteristic, which reflects how tightly the repeated measurements are clustered around the mean.

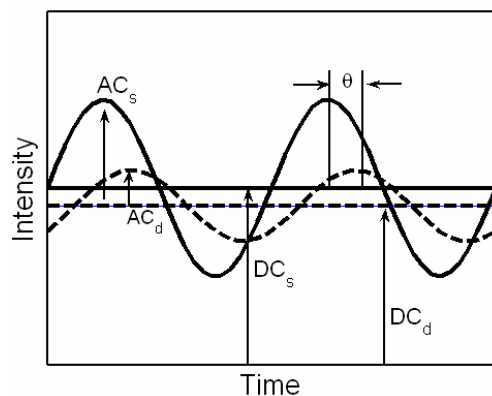


Fig. 2 Frequency domain model of data acquisition. AC is the amplitude of the modulation and DC is the average intensity, where the subscripts *s* and *d* denotes the source (solid line) and detector (dashed line), respectively.  $\theta$  represents the phase shift between the two signals.

Typically, the NIR light in a tissue medium tends to exponentially decay with increasing source-detector separation. In frequency-domain measurements, it is expected that fluorescence signal in terms of modulation depth (AC/DC) and  $\theta$  varies linearly with respect to the source-detector distance. As the fluorescence signal decays exponentially with increasing sources-detector distance, the magnitude of standard deviation values in AC and  $\theta$  also tend to decrease accordingly. This is contradictory to the SNR (signal-to-noise ratio), which is expected to decrease at detectors far from the source locations. In order to reflect the true correlation of measurement errors with respect to source-detector separation and remain consistent with the SNR behavior, the repeated measurements of AC and  $\theta$  were normalized prior to calculating the standard deviation values.

The statistical parameters (mean and standard deviation  $\sigma$ ) of five normalized measurements were calculated as below (*x* can be any AC or  $\theta$ );

$$\bar{x} = \sum_{n=1}^5 x_n \quad (1)$$

$$\sigma = \sqrt{\frac{\sum_{n=1}^5 (x_n - \bar{x})^2}{5-1}} \quad (2)$$

Following the correlation studies, only the uncorrelated parameters were considered as noise pre-filtering tools, and appropriate cut-off values estimated (described in Section 3.1). These uncorrelated parameters were in turn used in different combinations in order to develop different noise pre-filtering techniques towards tomography studies.

### 2.3.1 Model mismatch error

The performance of different noise pre-filtering techniques was evaluated using the model mismatch errors. These errors are defined as the difference between the experimental measurements (after pre-filtering the noisy measurements) and simulated measurements of AC and  $\theta$ . The simulated measurements were obtained by solving the coupled diffusion equations, which describes light propagation and fluorescence generation in a turbid medium, using the Galerkin approximation of the finite element method (FEM) [20-21]. The experimental fluorescence measurements were referenced for each given point source illumination, in order to account for the instrument effects [14]. The simulated measurements

data were also referenced accordingly and the model mismatch error in terms of logarithmic AC ratio ( $\ln(\text{ACR})$ ) and relative phase shift (RPS) were determined by:

$$\text{ACR}_{\text{error}} = \ln(\text{ACR})_{\text{exp}} - \ln(\text{ACR})_{\text{sim}} \quad (3)$$

$$\text{RPS}_{\text{error}} = \text{RPS}_{\text{exp}} - \text{RPS}_{\text{sim}} \quad (4)$$

where ACR and RPS are the referenced AC (AC ratio) and phase shift (relative phase shift) [14]. In these model mismatch studies, the experimental and simulated fluorescence measurements were referenced after pre-filtering the noisy measurements using the developed noise pre-filtering techniques.

#### 2.4 Image reconstructions

A computationally efficient version of the approximate extended Kalman filter (AEKF) [22, 23] was used to reconstruct the 3-D fluorescence absorption coefficient ( $\mu_{\text{axf}}$ ) distribution in the breast phantom. The AEKF is a weighted-damped non-linear least-squares optimizer, weighted by the inverse of the sum of the measurement and model error covariance matrices and damped by the inverse of the recursively updated parameter error. This Bayesian method regularizes the inversion in an optimal manner, and explicitly compensates for spatial variability in SNR. Measurement error variances were assumed uncorrelated, with variances experimentally determined for repeated observations (we used 5) for each source-detector pair. Model error variances were also assumed uncorrelated, and were empirically chosen to be one-fourth the mean of the measurement error variance (as in [16,23]) in order to regularize underdetermined parts of the system. Reconstructions were performed with initial guess in the unknown parameter ( $\mu_{\text{axf}}$ ) that was assumed to be homogeneous with a low value of  $0.003 \text{ cm}^{-1}$  for the entire phantom. These parameter values were then transformed prior to updates using pseudo-beta transforms [22] in order to bounds-constrain parameter updates to within feasible values; initial transformed parameter error variance was empirically estimated to be 0.01 (as in [14]). Extensive details of the algorithm are presented elsewhere [14-17, 22, 23].

The reconstruction process was carried out recursively until the system converged to less than 1% in sum of squared prediction error or when 50 iterations has been reached. Anterior and lateral views of the 3-D reconstructed phantom under the perfect and imperfect uptake cases were plotted using Tecplot 10.6 software (Tecplot Inc., Bellevue, WA). A cutoff value of fluorescence absorption coefficient,  $\mu_{\text{axf}}$  was selected to distinguish between the background and the target based on the break between modes in the histogram of the reconstructed  $\mu_{\text{axf}}$  [14]. The reconstructed targets are quantified in location and the distance-off. The Euclidean distance between the value-weighted centroids of the predicted and actual target location was termed as distance-off. The reconstructed optical contrast was estimated as the ratio of the mean of fluorescence absorption coefficient in reconstructed target to that in the background.

### 3. Results and discussion

#### 3.1 Correlation of different measurement parameters

Correlation studies were performed among the following measurement parameters as described in Section 2.3. The homogeneous experimental data of AC/DC, phase shift ( $\theta$ ), measurement errors in AC and  $\theta$  were plotted with respect to the source-detector distance, since these measurement parameters tend to change with source-detector distance.

Figure 3(a) shows that the logarithm of modulation depth varied linearly with respect to source-detector distance, verifying that the modulation depth decreases exponentially with increasing source-detector distance (based on the physics of light decay). The linear

correlation was observed only up to a source-detector distance of 8.0 cm (based on statistical regression analysis,  $R^2=0.76$ ) and hence measurements beyond source-detector distance of 8.0 cm can be considered noise. From past studies performed by Godavarty *et al.* [14], the model mismatch error was significantly larger for those source-detector pairs (or measurement points) whose modulation depth was  $<0.025$ . Using this as an initial basis for our studies, the noisy measurements filtered using the 8.0 cm source-detector distance cut-off were a subset of the noisy measurements filtered using modulation depth of 0.025 as cut-off. However, beyond a source-detector distance of 6.0 cm, it was observed that the maximum modulation depth was less than 0.025. Hence, measurements even beyond source-detector distance of 6.0 cm can be considered as noise, although the linear correlation between the logarithm of AC/DC still exists at this source-detector distance.

From plotting the phase shift with respect to the source-detector distance (Fig. 3(b)), it was observed that the phase shift deviates from the linear trend as the source-detector distance is  $\sim \geq 6.0$  cm and source-detector distances of  $\leq 1$  cm. From simulated phase measurements under similar experimental conditions, it was observed that such deviations are possible probably due to the curvature of the tissue phantom and the sinusoidal nature of the phase measurements (see Fig. 3(c)). It was thus difficult to differentiate between actual phase measurements and noise, causing phase shift to be an inappropriate noise pre-filtering criteria in our studies. The standard deviations of normalized phase shift were observed to be independent of the source-detector distance (Fig. 3(d)) and also  $< 1\%$ . Hence this measurement parameter was not considered as a significant parameter to filter noisy measurements.

Figure 3(e) shows that the measurement error in AC (i.e. standard deviation of normalized amplitude) increases linearly with the source-detector distance. When 20% of the standard deviation of normalized amplitude was chosen as a cut-off, the eliminated measurements become a subset of the measurements filtered using modulation depth of 0.025 as cut-off (as shown in Fig. 3(f)). However, a 20% of the standard deviation represents a very high tolerance to measurement error (close to the maximum standard deviation value). Therefore, in our studies, a 10% of the standard deviation of normalized amplitude ( $\sim 50\%$  of the maximum value) was selected as the maximum deviation in measurements that can be tolerated for tomographic imaging. The noisy measurements eliminated using the 10% cut-off value in measurement error of AC were not the same set of measurements eliminated using the modulation cut-off value of 0.025. This in turn implies that modulation depth are not correlated to measurement errors in AC, thus considering the measurement error in AC as another noise pre-filtering criterion during image reconstructions.

In summary, based on the correlation studies among different measurement parameters, modulation depth and measurement error in AC were chosen as the two noise pre-filtering criteria for tomography studies. These noise pre-filtering tools were used in different combinations to develop different noise pre-filtering techniques (PFT), as follows: (i) PFT-1 using only modulation depth (cut-off 0.025) as the noise pre-filtering tool (PFT-1); (ii) PFT-2 using only measurement error in AC (10% cut-off) as the noise pre-filtering tool; and (iii) PFT-3 using both the modulation depth and measurement error in AC as the noise pre-filtering tools.

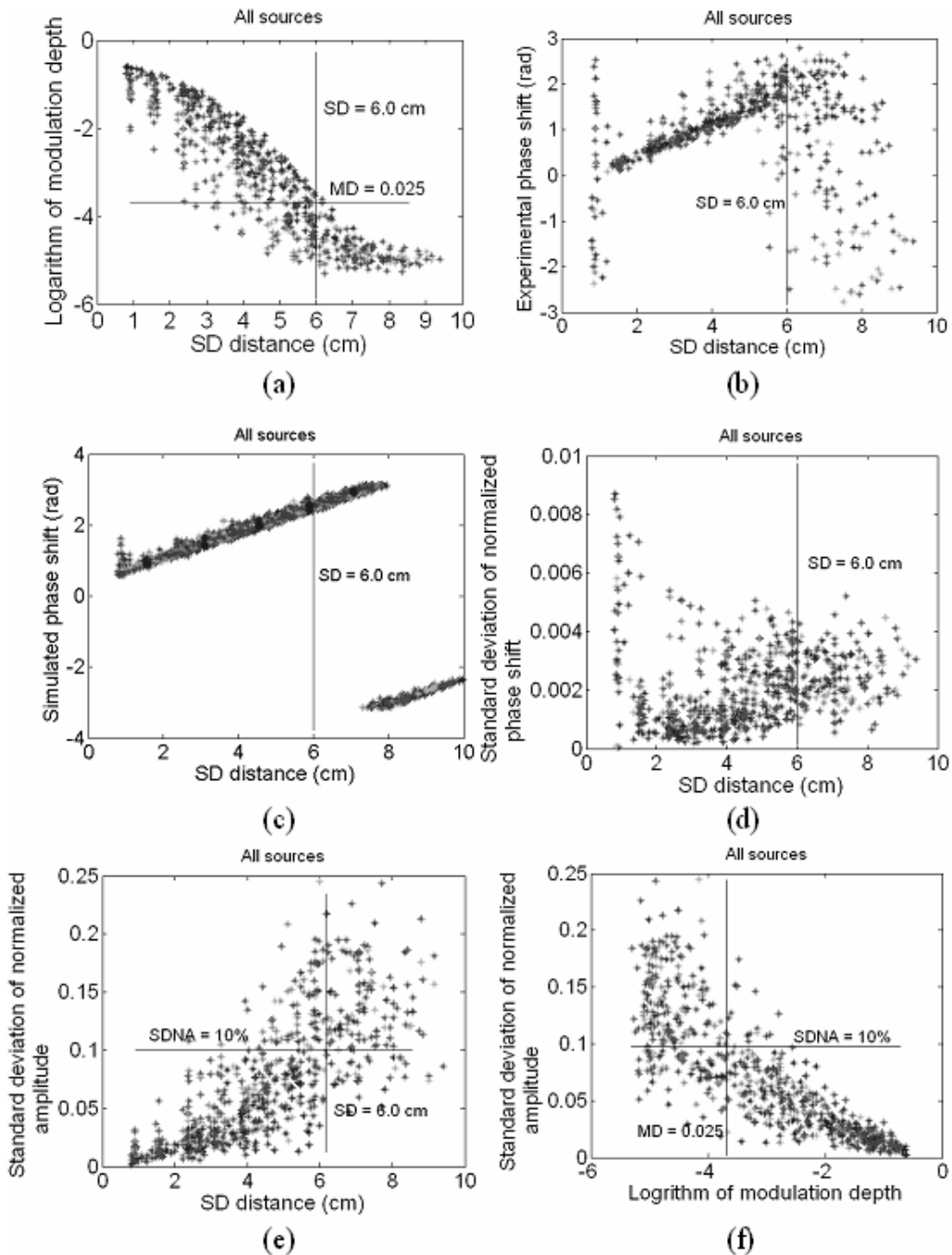


Fig. 3. Correlations of different measurement parameters from experimental measurements of homogenous phantoms. Here SD represents source-detector distance MD is the modulation depth; and SDNA represents the standard deviation of normalized amplitude. (a) Logarithm of modulation depth vs SD distance, (b) Phase shift vs SD distance, (c) Phase shift from simulated studies vs SD distance, (d) Standard deviation of normalized phase shift vs SD distance, (e) Standard deviation of normalized amplitude (SDNA) vs SD distance, and (f) SDNA vs logarithm of modulation depth.

The effects of the three noise pre-filtering techniques were assessed with respect to no noise pre-filtering technique (i.e. No PFT) employed on measurements, in terms of model mismatch error and the quality of 3D image reconstructions.

### 3.2 Model mismatch error studies

Model mismatch errors are represented as the variance ( $\sigma^2$ ) of  $\ln(\text{ACR})$  and RPS using the different noise-filtering techniques (i.e. No PFT, PFT-1, PFT-2, PFT-3) under perfect (1:0) and imperfect (100:1) uptake cases, in Fig. 4 and 5, respectively. In most experimental cases of varying fluorescence absorption contrast ratios (1:0 and 100:1) and target depths (1.4, 2.0 and 2.8 cm), the application of noise pre-filtering techniques tends to improve the model

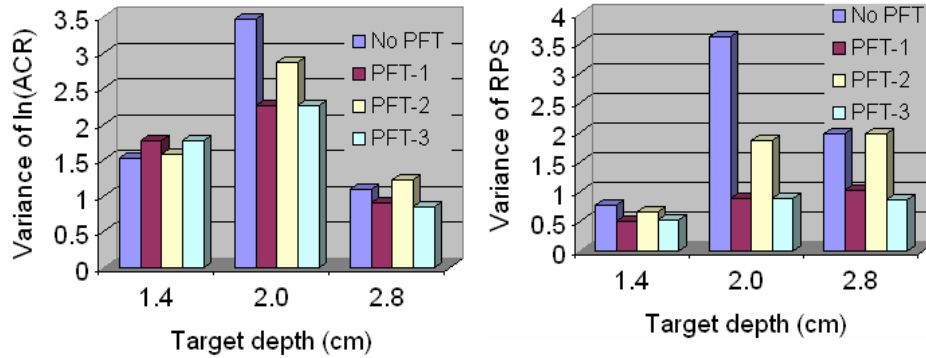


Fig. 4. Variances of model mismatch error in (a)  $\ln(\text{ACR})$  and (b) RPS for different target depths (1.4, 2.0, 2.8 cm) with 1:0 absorption optical contrast ratio under different pre-filtering techniques.

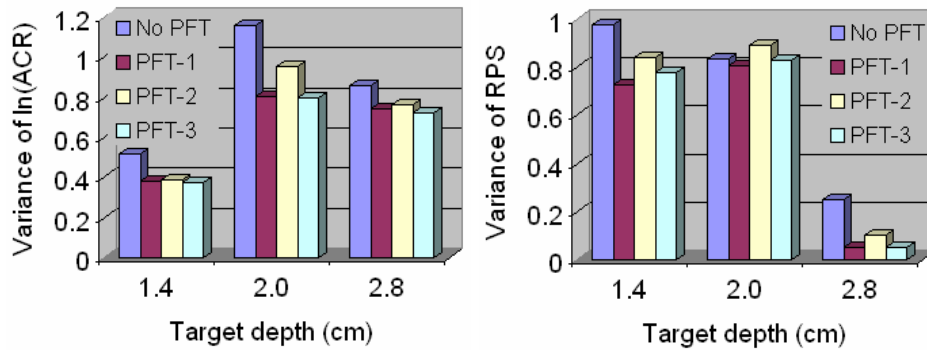


Fig. 5. Variances of model mismatch error in (a)  $\ln(\text{ACR})$  and (a) RPS for different target depths (1.4, 2.0, and 2.8 cm) with 100:1 absorption optical contrast ratio under different pre-filtering techniques.

match in comparison to the no PFT case. This indicates that at least some of the model mismatch errors in the no PFT case is due to noisy measurements that were filtered using the three PFTs. Comparing the results among the three PFTs, it was observed in most cases that employing PFT-1 or PFT-3 provided relatively smaller variance in model mismatch errors of both AC and phase shift in comparison to the variance obtained by employing PFT-2. Unlike in PFT-2, where measurement error in AC alone was the criteria for pre-filtering noisy data, PFT-1 and PFT-3 employed modulation depth as a noise pre-filtering criteria. This implies

that modulation depth based pre-filtering is probably a better criteria in reducing the model mismatch errors in comparison to the measurement error in AC based criteria.

### *3.3 Image reconstructions*

Three-dimensional image reconstructions were performed using the different noise pre-filtering techniques (no PFT, PFT-1, PFT-2, PFT-3) for different target depths (1.4, 2.0 and 2.8 cm) and fluorescence absorption contrast ratios (1:0 and 100:1). For brevity, only the results from the experimental case with target depth of 2.8 cm under perfect (1:0) and imperfect (100:1) uptake contrast ratios cases are presented in Fig. 6 and 7, respectively.

Under perfect uptake conditions (i.e., no background fluorescence), the contamination of measurements with background noise is relatively low and reconstructions were thus largely artifact free, regardless of the pre-filtering technique (Fig. 6, Table 3). Similarly, even with imperfect uptake (target:background contrast of 100:1), there was no significant effect of noise pre-filtering techniques on quality of reconstruction when target depths were relatively shallow (i.e. 1.4 cm and 2.0 cm deep) (see Table 4). However, for the deepest targets (2.8 cm deep) under imperfect uptake conditions, artifacts appeared within the reconstructed images when no PFT case was applied (see Fig. 7(a)). The artifacts were reduced upon employing the noise pre-filtering techniques as seen from Fig. 7(b)-(d). These preliminary results suggest that pre-filtering of noise may only become crucial when targets are deep and there is confounding fluorescence in the background. It should be noted that we also performed image reconstructions (not shown here for brevity) using modulation depth cut-off values of 0.015 and 0.035 (in PFT-1). The higher cut-off value (0.035) reduced the quality of the

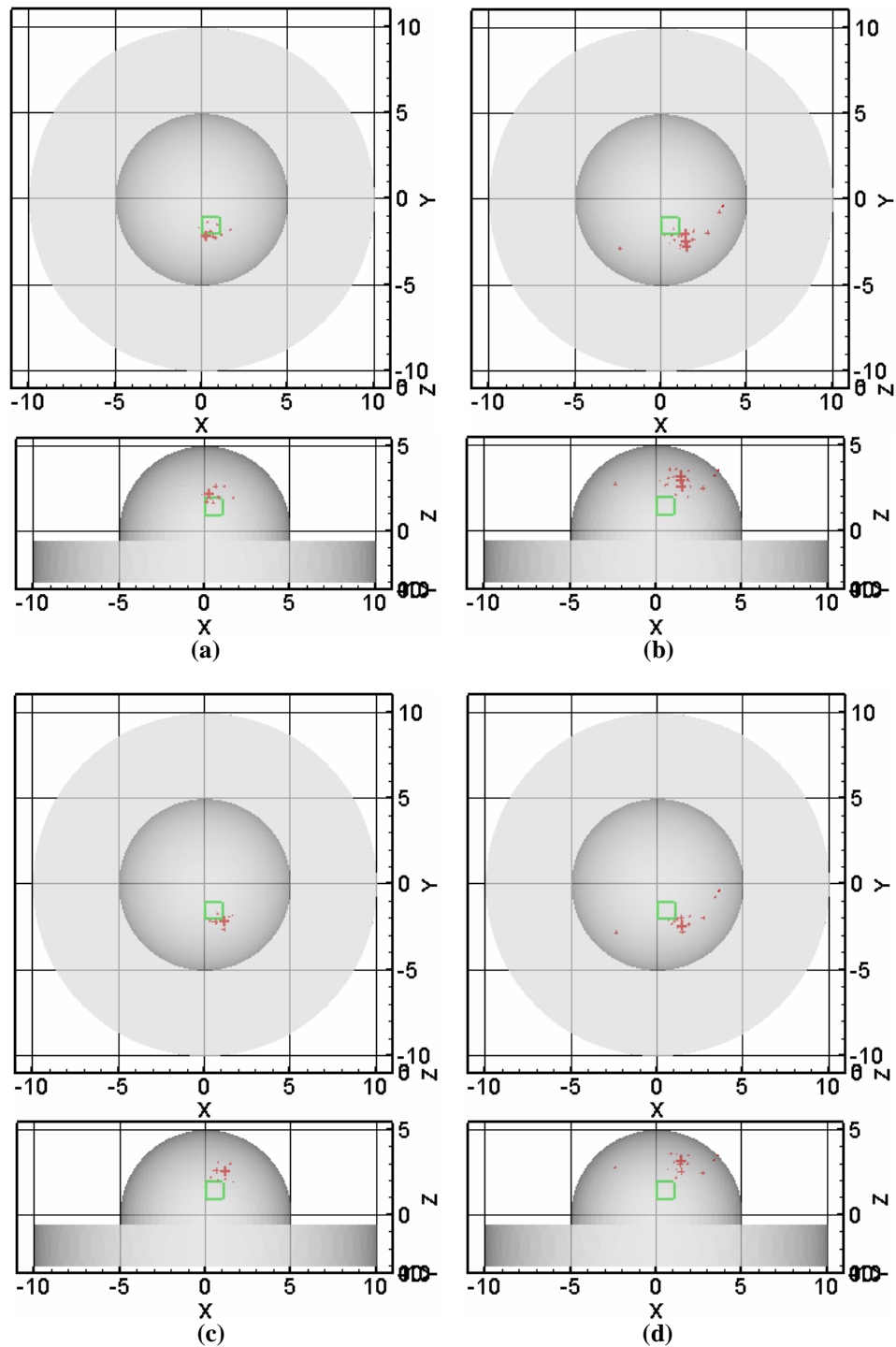


Fig. 6. Anterior (x-y) and lateral views of reconstructed images of the breast phantom under perfect uptake case (1:0) and target located 2.8 cm deep obtained using different noise pre-filtering techniques: (a) no cut-off, (b) PFT-1, (c) PFT-2, and (d) PFT-3. The size of red '+' symbols is directly proportional to the intensity of the reconstructed parameter  $\mu_{axf}$ . The green pane indicates the true location of the targets

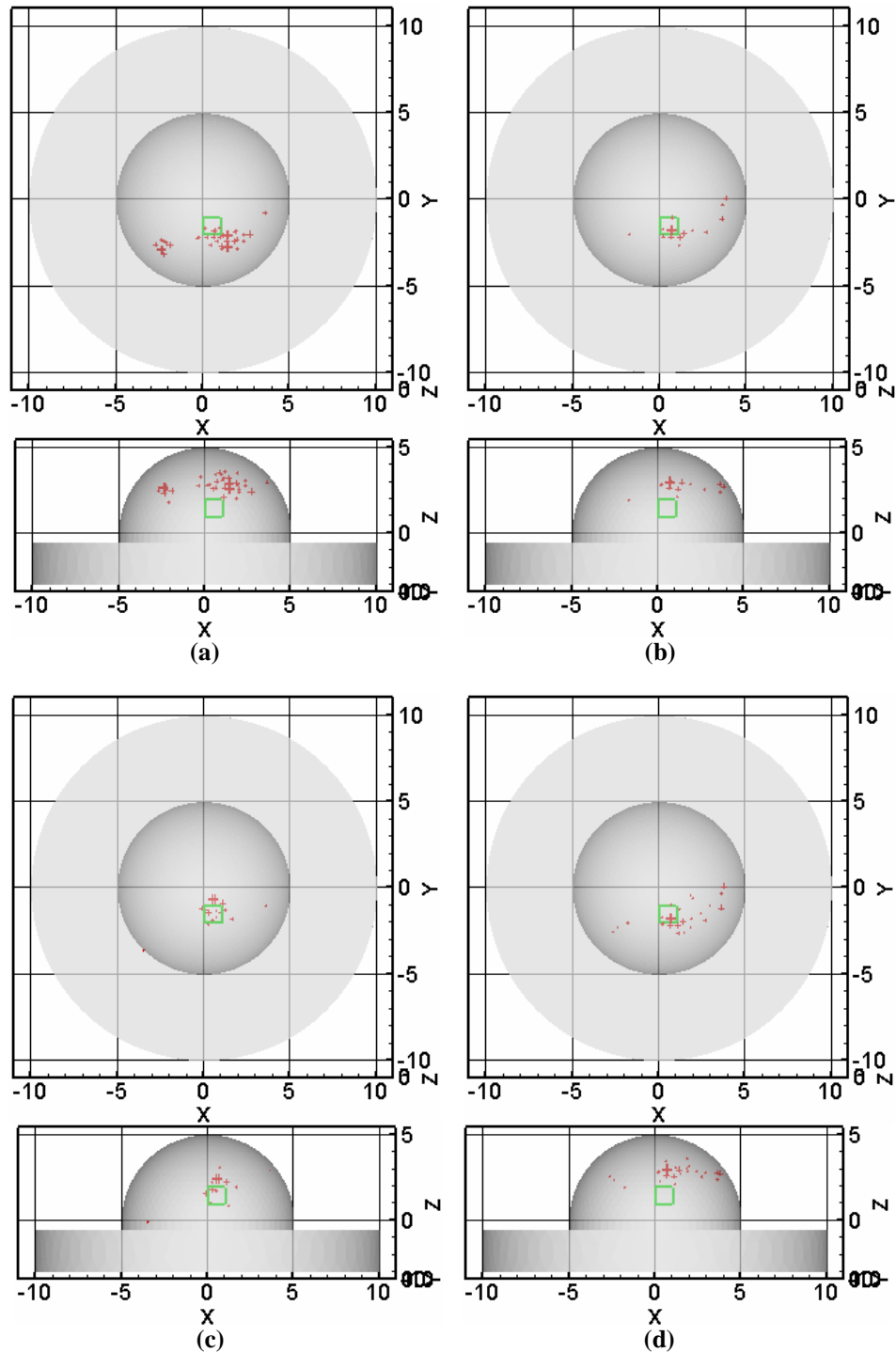


Fig. 7. Anterior (x-y) and lateral views of reconstructed images of the breast phantom under imperfect uptake case (100:1) and target located 2.8 cm deep obtained using different noise pre-filtering techniques: (a) no cut-off, (b) PFT-1, (c) PFT-2, and (d) PFT-3. The size of red '+' symbols is directly proportional to the intensity of the reconstructed parameter  $\mu_{asf}$ . The green pane indicates the true location of the targets.

reconstructions for the deepest target. This is probably from pre-filtering more useful measurements upon using larger modulation cut-off values, in experimental cases with no background fluorescence. There was no significant impact on the quality of image reconstructions at modulation depth cut-off value of 0.015. However, upon further decreasing the cut-off value, the noisy measurements generated artifacts especially in deeper targets with background fluorescence. It was also observed that the effect of PFTs on model mismatch errors was almost independent of their effect on the quality of image reconstructions in these studies.

The quantified results of the target localization and optical contrast are provided in Tables 3 and 4 for the perfect and imperfect uptake cases, respectively. In all the experimental studies (1:0 and 100:1 cases), the target localization and the recovered optical contrast improved upon using PFT-2 in comparison to using PFT-1 and PFT-3. In most cases, the target localization for the no-PFT case was good and comparable to the target localization using the PFT-2 case, as observed from Tables 3 and 4. However, the reconstructed images using the no-PFT generated artifacts at deeper target cases contaminated by background noise, which were eliminated by PFT-2 case. In addition, it was also observed there was no correlation in the drop in model mismatch errors using noise PFTs and the quality of image reconstructions. These observations are preliminary and will be validated by extensive tomography studies in the future.

Table 3 Quantitative analysis of reconstructed target using different noise pre-filtering techniques for the perfect uptake case (1:0)

Target depth (cm)	Filtering techniques	Numbers of measurements used in reconstructions	Centroid		Distance off (cm)	Optical contrast
			True value [x y z] cm	Reconstructed [x y z] cm		
1.4	No cut-off	320	[0.5 -2.5 2.5]	[0.71 -2.33 2.57]	0.28	114.6
	PFT-1	126		[0.53 -2.26 2.58]	0.25	104.6
	PFT-2	220		[0.72 -2.33 2.55]	0.29	114.8
	PFT-3	125		[0.53 -2.26 2.58]	0.25	104.5
2.0	No cut-off	512	[0.5 -1.5 2.5]	[0.77 -1.74 2.95]	0.58	73.6
	PFT-1	188		[0.79 -1.76 3.04]	0.67	100.0
	PFT-2	265		[0.78 -1.77 3.03]	0.65	65.5
	PFT-3	183		[0.80 -1.76 3.04]	0.67	100.0
2.8	No cut-off	576	[0.5 -1.5 1.5]	[0.45 -1.94 2.21]	0.84	42.0
	PFT-1	154		[1.25 -2.09 2.99]	1.77	11.8
	PFT-2	284		[0.86 -2.05 2.61]	1.29	35.4
	PFT-3	143		[1.32 -2.07 3.04]	1.83	15.6

Table 4 Quantitative analysis of reconstructed target using different noise pre-filtering techniques for the imperfect uptake case (100:1)

Target depth (cm)	Filtering techniques	Numbers of measurements used in reconstructions	Centroid		Distance off (cm)	Optical contrast
			True value [x y z] cm	Reconstructed [x y z] cm		
1.4	No cut-off	704	[0.5 -2.5 2.5]	[0.58 -2.24 2.60]	0.29	10.7
	PFT-1	401		[0.01 -2.30 2.54]	0.53	10.1
	PFT-2	440		[0.87 -2.27 2.62]	0.45	13.5
	PFT-3	371		[0.01 -2.31 2.54]	0.54	10.0
2.0	No cut-off	896	[0.5 -1.5 2.5]	[0.27 -1.69 3.08]	0.65	37.1
	PFT-1	480		[0.75 -2.04 3.08]	0.83	14.5
	PFT-2	585		[0.64 -2.02 3.05]	0.77	18.4
	PFT-3	458		[0.81 -2.06 3.07]	0.86	13.7
2.8	No cut-off	768	[0.5 -1.5 1.5]	[0.38 -2.22 2.85]	1.53	9.4
	PFT-1	480		[1.46 -1.49 2.82]	1.63	34.8
	PFT-2	548		[0.44 -1.29 1.89]	0.45	92.3
	PFT-3	460		[1.29 -1.53 2.84]	1.55	26.8

Parallel to the above observations, an interesting observation was made for all experimental cases of 1:0 and 100:1 contrast ratios, and varying target depths. Image reconstructions with and without the use of noise pre-filtering techniques, consistently generated target(s) close to the true target location (see Fig. 6 and 7). However, the artifacts appeared at different locations in the reconstructed images using different pre-filtering techniques. In a real clinical environment, the true location and number of targets (or tumors) are unknown. Hence by combining image reconstructions using different noise pre-filtering techniques, we could possibly differentiate the target (from its consistent appearance in the same location for each reconstructed case) from artifacts (whose location is random and tends to change based on the noise pre-filtering technique employed), thus improving the accuracy of target detectability. In other words, this approach may help minimize the false positive and true negative cases during ROC (receiver operator characteristic) analysis.

#### 4. Conclusions

Noise plays a significant role in any experimental study in any given field of research. Differentiating the acquired measurement as a weak signal or noise is very crucial in the post-processing and analysis of the data. Imaging studies in a real clinical environment, data analysis can significantly impact the radiologist's report on the subject's health condition and eventually the treatment procedure. Fluorescence-enhanced optical imaging is an emerging technology towards cancer diagnostic/prognostic imaging. To date, there is still a need to develop standardized methods to differentiate noise from true optical signals.

The current work is a preliminary study towards developing appropriate noise pre-filtering techniques, such that the reconstructed images of the imaged tissue medium or phantoms have minimal artifacts or the artifacts can be easily differentiated from the actual target(s) locations. In this contribution, we have studied the correlations of different measurement parameters obtained from large homogeneous breast phantoms using the FDP-ICCD imaging system. Based on the correlations of these measurement parameters, three noise pre-filtering techniques were chosen for removing the noisy measurements (employing AC/DC and measurement error in AC). From the perfect and imperfect uptake

studies under varying target depths, it was observed that the noise pre-filtering techniques become significant in cases where the target is deeply located ( $> 2$  cm) and when fluorescence is also present in the background. Interestingly, performing 3-D image reconstructions using all the different proposed noise pre-filtering techniques (no PFT, PFT-1, PFT-2, and PFT-3) can possibly differentiate target(s) from artifacts. This observation was based on the fact that the target(s) repeatedly reconstructed in the same location using either of the noise pre-filtering technique, whereas the location of artifacts varied with the technique employed. This result is very significant, especially from a clinical perspective of trying to minimize false positive cases.

The performance of these noise pre-filtering techniques will be further verified and validated by extensive future testing under varying experimental conditions from measurements obtained at different target depths, target number, target volumes, fluorescence absorption contrast ratio in large and clinically relevant tissue volumes and using different cut-off values in the noise pre-filtering parameters (modulation depth and standard deviation in normalized amplitude).

In addition, the developed noise pre-filtering techniques were from experimental results obtained using a particular type of imaging system, which employed modulated laser diodes (source) and ICCD camera (detector) along with pertinent electronics. The magnitude and sources of measurement noise may vary for different imaging systems, based on the instrument developed and its sensitivity. Hence, these noise pre-filtering techniques need to be assessed on various imaging systems with initial studies employing different cut-off values of the un-correlated parameters, before the conclusions can be safely generalized. Similarly, the effect of the inversion algorithm employed in conjunction with the noise pre-filtering techniques will be assessed in the future.